J. Fluid Mech. (1989), *vol.* 208, *pp.* 67–89
Printed in Great Britain

Linear instability of the wake behind a flat plate placed parallel to a uniform stream

By D. T. PAPAGEORGIOU[1] AND F. T. SMITH[2]

[1] Department of Chemical Engineering, City College of New York, Convent Avenue and 140th Street, New York, NY 10031, USA

[2] University College London, Department of Mathematics, Gower Street, London WC1 E6BT, UK

(Received 11 September 1987 and in revised form 14 March 1989)

The growth of linear disturbances in the high-Reynolds-number laminar wake of a flat plate aligned with a uniform stream is investigated. The theory is developed rationally by use of appropriate wake profiles which originate at the trailing edge as double Blasius distributions and thereafter satisfy the equations of motion, in contrast to previous theoretical work where model profiles are used. We also emphasize the structures and scales of the instability in order to provide a rational basis for the development of nonlinear analyses as opposed to existing *ad hoc* ones. Disturbances, in the near wake, respond according to the Rayleigh equation which is considered analytically for short-, long- and neutral-wave solutions. For more general stability characteristics eigensolutions must be obtained numerically. We calculate these at successive wake stations for 'improved' basic flow profiles which are obtained as solutions of the wake boundary-layer equations. Our numerical results indicate fairly good agreement with the asymptotic theory and some experimental data (see §7).

1. Introduction

In recent years there has been an increasing interest in wake flows at high Reynolds numbers. Such wakes are a common occurrence and are significant in many physical situations, the main application being to aerodynamics. In general, these flows are unstable in reality and it is desirable, therefore, to obtain a clear theoretical understanding of the linear and nonlinear instability mechanisms involved. This work is concerned with the high-Reynolds-number motion in the wake of bodies that are sufficiently streamlined that attached motion results on the body surface and a thin viscous wake is formed just downstream. The case of non-streamlined motion, with large-scale separation, is a related but different problem. For simplicity the motion considered is that of an infinitely thin aligned flat plate (of finite length) travelling with uniform speed in a viscous incompressible fluid. The Reynolds number for the flow is large.

Careful experimental work (Sato & Kuriki 1961; Miksad *et al.* 1982; Miksad, Jones & Powers 1983) tends to indicate that disturbances evolve linearly and two-dimensionally in the near wake. Furthermore, the subsequent development of the wake downstream is observed to be greatly influenced by such initial disturbances. This suggests that the evolution of the wake might be manipulated in a favourable way physically, and it seems important, therefore, to possess a quantitative theoretical knowledge of the initial evolution of linear fluctuations.

The steady basic flow just downstream of the sharp trailing edge of a flat plate can be divided into the flow in a thin viscous wake and, outside, a uniform incompressible main stream. The flow in the thin wake is governed by the boundary-layer equations and in the near wake is described in an important paper by Goldstein (1930). This is done by means of asymptotic solutions for small distances from the trailing edge; these were later shown to match, in a consistent manner, to the flow just upstream of the trailing edge by means of viscous–inviscid interaction in the 'triple deck' structure (see, Stewartson 1969; Messiter 1970).

Owing to the complicated nature of the unperturbed steady flow, there have been very few theoretical investigations of wake stability assuming the correct wake features. Previous investigators have used only model basic-flow profiles (e.g. of Gaussian or sech^2 form) and have computed growth rates and frequencies at the position where the model profile roughly corresponds to the physical flow (see Hollingdale 1940; McKoen 1957; Sato & Kuriki 1961; Mattingly & Criminale 1972). Strictly the Gaussian or sech^2 profiles are not correct for the majority of the wake since they are, after all, far-wake properties only. Instead the wake profiles should be obtained numerically (with a double Blasius profile at the start), from the boundary-layer equations, and this is the course we follow.

Curle (1957) and Taneda (1965) attempted to find a neutral curve, and thus a minimum Reynolds number above which instability first sets in, from solutions of the Orr–Sommerfeld equation. These calculations are not entirely satisfactory, however, owing to the non-parallelism of the flow in the near wake at $O(1)$ Reynolds numbers. A strictly better approach, which is adopted here, appears to be the use of Rayleigh's equation together with the quasi-parallel form of the basic flow, for high Reynolds numbers. In this work we present some asymptotic solutions of the Rayleigh equation which we feel correspond more to the physical situation. Of interest, therefore, is the work on stability of parallel unbounded inviscid flows. Drazin & Howard (1966) considered the long-wave limit and produced some general results that can be applied, under certain assumptions, to wakes, jets and shear layers. Later in the paper (see §4) we tackle this limit from a different point of view for the wake case.

The strategy adopted in the rest of the paper is as follows. Here two-dimensional instability theory seems a quite reasonable starting point for the present rational approach, partly because it is slightly less complicated than three-dimensional theory and partly because the work is found to yield predictions (see below) which tend to be consistent overall with the experimental evidence available: see also earlier comments on two-dimensionality in the experiments. In §2 the linear stability problem is formulated and the choice of scales that lead to the Rayleigh equation is noted. In §3 the behaviour of short waves (short compared with the boundary-layer thickness) is examined. In §4 long-wave disturbances, long compared with the boundary-layer thickness but still shorter than the plate length, are considered. In §5 neutral waves are found for the Goldstein-type velocity profiles that hold in the near wake, where in effect the inviscid disturbances originate: see also later remarks. In §6 the numerical method used to solve the Rayleigh equation, together with the calculation of basic velocities, is described. Stability calculations are performed for basic flow profiles which are solutions of the boundary-layer equations with wake boundary conditions that hold in a thin viscous wake downstream of the trailing edge. These profiles are nominally exact, and the empiricism involved in the determination of the unperturbed flows in previous studies does not arise. In §7 the

results are presented and compared with experiments and previous model-profile calculations.

Throughout this paper, the origin of Cartesian coordinates is fixed at the trailing edge with x, y the streamwise and transverse coordinates respectively. The Reynolds number is denoted by R_e and is assumed to be asymptotically large. Also u, v, p are the velocities in the x-direction, y-direction and the pressure respectively, and ψ is taken to be the stream function for the two-dimensional flow.

2. Formulation of linear stability problem

When the fluid leaves the trailing edge, the laminar boundary layers from either side of the plate merge and are accelerated to form a thin wake. The thickness of the wake is of order $R_e^{-\frac{1}{2}}$ and the motion is governed by the two-dimensional boundary-layer equations. The leading-order contribution to the velocity in the x-direction is symmetric about the wake centreline ($y = 0$) and has zero y-derivative at $y = 0$. Flow quantities in general have to be obtained numerically although they can be found in the near wake by means of the asymptotic expansions of Goldstein (1930) which are used here to represent the unperturbed flow field in some later analysis. It should be noted, therefore, that the disturbances covered here initially evolve in the vicinity of the trailing edge, a setting that is in line with experimental observations (see introduction).

Formally, then, small perturbations in the flow quantities are introduced in the wake beyond the trailing edge, but still outside the interactive triple-deck region (i.e. $x \gg R_e^{-\frac{3}{8}}$). The disturbances are expected to evolve inviscidly and so their x and y scales are equal. Also it is reasonable, from a physical point of view, to study fluctuations inside the thin wake; thus the scales are $x \sim y \sim R_e^{-\frac{1}{2}}$. It is convenient to introduce an order-one parameter α such that $x \sim y \sim R_e^{-\frac{1}{2}}\alpha^{-1}$. Physically α is the wavenumber of the disturbance when the wake thickness is scaled out. With this set-up in mind, let us now verify the conditions under which the Rayleigh stability equation ((2.1) below) is valid.

The starting point is the two-dimensional Navier–Stokes equations. The basic flow at a fixed x-station is two-dimensional and can be written as $(\bar{u}(y), 0)$, to leading order, where $\bar{u}(y)$ is quantified later on. On linearization about this basic state the equations become

$$u_t + \bar{u}u_x + v\bar{u}_y = -p_x + \frac{1}{R_e}(u_{xx} + u_{yy}),$$

$$v_t + \bar{u}v_x = -p_y + \frac{1}{R_e}(v_{xx} + v_{yy}),$$

$$u_x + v_y = 0.$$

The instability regions considered in this work have the scales mentioned above, and so the following coordinate changes are made:

$$x = R_e^{-\frac{1}{2}}\alpha^{-1}X, \quad y = R_e^{-\frac{1}{2}}\alpha^{-1}y_1, \quad t = R_e^{-\frac{1}{2}}\alpha^{-1}T.$$

Substitution into the linearized Navier–Stokes equations and rearrangement of terms then gives

$$u_T + \bar{u}u_X + v\bar{u}_{y_1} = -p_X + R_e^{-\frac{1}{2}}\alpha(u_{XX} + u_{y_1y_1}),$$

$$v_T + \bar{u}v_X = -p_{y_1} + R_e^{-\frac{1}{2}}\alpha(v_{XX} + v_{y_1y_1}),$$

$$u_X + v_{y_1} = 0.$$

So for the Rayleigh equation to be valid (i.e. for viscous terms to be negligible) the ordering $\alpha \ll R_e^{\frac{1}{2}}$ must be observed. For long waves, viscosity will become important when $\alpha \sim R_e^{-\frac{1}{2}}$, in which case there is an instability region having an order-one lateral and transverse extent, with a free viscous wake layer of thickness $R_e^{-\frac{1}{2}}$ embedded within it (see also Papageorgiou & Smith 1988). In the analysis that follows α obeys the inequality $R_e^{-\frac{1}{2}} \ll \alpha \ll R_e^{\frac{1}{2}}$. Further, since $\bar{u}$ varies on the $O(1)$-scale in x and the corresponding $\bar{v}$ is $O(R_e^{-\frac{1}{2}})$, the above demonstrates that the non-parallel flow effects are of higher order, relatively of $O(R_e^{-\frac{1}{2}})$ for α of order unity, as is usual in Rayleigh-type analysis.

The Rayleigh equation is derived by the introduction of a stream function and a normal-mode analysis. More specifically, the stream function is taken to be $\tilde{\psi}(X, y_1, T) = \psi(y_1)\exp(\mathrm{i}\alpha(X-cT))$, where c is the wave speed of the plane wave under consideration; substitution into the scaled linearized and inviscid Navier–Stokes equations above gives the classical Rayleigh stability equation

$$(\bar{u}-c)(\psi''-\alpha^2\psi) = \bar{u}''\psi \quad \text{with} \quad \psi(\pm\infty) = 0. \tag{2.1}$$

The boundary condition on ψ ensures decay of the disturbance at the edges of the wake. Two important limits are most amenable to analysis and are considered in the next sections. These are $\alpha \to \infty$ and $\alpha \to 0$, which correspond to the evolution of short- and long-wave disturbances respectively. Numerical solutions of (2.1) above are presented in §6.

3. Short waves, $\alpha \to \infty$

Even though it does not seem possible to obtain analytical solutions of (2.1) for general values of α, an asymptotic description of the solutions for $\alpha \to \infty$ and $\alpha \to 0$ can be constructed and thus a good idea of the scale of instability can be gained. Such asymptotic analyses have been considered by previous authors but for model underlying basic flows alone. Here we study the instability of proper wake profiles and in particular we want to emphasize the structures and scales involved in order to guide later nonlinear work. In this section we address short waves, where $\alpha \to \infty$. Physically, the waves are short compared with the wake thickness.

Inspection suggests the following expansions in the compressed region $y = \alpha^{-1}y_1$ with $Y = O(1)$:

$$c = c_0 + \alpha^{-1}c_1 + \alpha^{-2}c_2 + \alpha^{-3}c_3 + \alpha^{-4}c_4 + \ldots, \tag{3.1a}$$

$$\bar{u} = \pm\alpha^{-1}\lambda Y + \lambda_4\alpha^{-4}Y^4 + \ldots \quad (Y \gtrless 0), \tag{3.1b}$$

$$\psi = \psi_0 + \alpha^{-1}\psi_1 + \alpha^{-2}\psi_2 + \alpha^{-3}\psi_3 + \ldots. \tag{3.1c}$$

Equation (3.1b) follows from the form of the Blasius distribution as $y \to 0$. (If $\bar{u} = f'(\zeta)$, $\zeta = y/x^{\frac{1}{2}}$, then $f''' + 1/2 f\, f'' = 0$ together with $f(0) = f'(0) = f'(\infty) - 1 = 0$. Numerical integration implies that $\lambda = f''(0) = 0.332\ldots$ and $\lambda_4 = -\frac{1}{48}\lambda^2 (< 0)$.) In the analysis that follows, the smoothing Goldstein zone, of thickness $x^{\frac{1}{3}}$, still looks thin compared with the lateral extent of the instability region since we consider instability wavelengths that satisfy $\alpha^{-1} \gg x^{\frac{1}{3}}$. Substitution of the expansions (3.1a–c) into (2.1), and balance of successive powers of α yields

$$\psi_0^{\pm} = A_0 \mathrm{e}^{\mp Y}, \tag{3.2}$$

where $\psi_0^{\pm}$ is the solution for $Y > 0$ and $Y < 0$ respectively. Next we find

$$\psi_1 = \psi_2 = 0, \quad c_0 = c_2 = c_3 = 0. \tag{3.3}$$

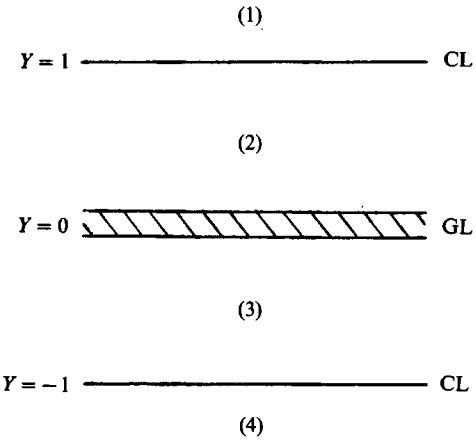

FIGURE 1. The various regions in which short waves develop. CL denotes a critical layer, and GL the Goldstein layer.

The solutions (3.3) follow from the fact that if c_0 is non-zero, then the equations satisfied by $\psi_0, \psi_1, \ldots$ are identical and by a renormalization trivial solutions would result. To avoid this (3.3) must hold. Solution (3.2) above reflects the continuity of mass flux in the fluid, to leading order, at $Y = 0$. The pressure must also be continuous to leading order and by use of the pressure equation

$$\mathrm{i}\alpha(\bar{u}-c)\,u - \mathrm{i}\alpha\psi\bar{u}' = -\mathrm{i}\alpha p \tag{3.4}$$

together with the solution (3.2), we find a value for c_1:

$$c_1 = \lambda. \tag{3.5}$$

The first important stage is at $O(\alpha^{-2})$ where the equation for ψ_3, together with its boundary condition, is

$$\psi_3'' - \psi_3 = \frac{12\lambda_4 Y^2 \psi_0}{\pm\lambda Y - c_1}, \quad \psi_3(\pm\infty) = 0. \tag{3.6}$$

The fact that c_1 is real shows that short-wave disturbances are almost neutral and have growth rates of order α^{-3} at most. In what follows we present uniformly valid asymptotic solutions that satisfy the boundary conditions; the $O(\alpha^{-3})$ growth rate is also calculated.

It can be seen from (3.5) that (3.6) has a singularity at the levels $Y = \pm 1$. These levels correspond to critical layers and the singularities can be smoothed out by the introduction of linear viscous layers in their vicinity. The net effect of these layers is to give the inviscid solution a phase jump of $-\mathrm{i}\pi\,\mathrm{sgn}\,(\bar{u}'(y = y_c))$, due to the logarithmic singularity there (see Drazin & Reid 1981; Lin 1955). So, in order to find a uniformly valid solution for ψ_3 we must consider solutions in each of the relevant physical regions shown in figure 1, and match solutions across them. Further matching with the Goldstein layer fixes the value of c_4.

The details of this analysis are given in Appendix A. Briefly then, we solve for ψ_3 in each of the regions (1), (2), (3) and (4). This produces six constants of integration (see Appendix A); four algebraic equations, connecting the constants, are obtained from the phase jumps across the critical layers and continuity of mass flux there. The

last two equations that enable complete solution are obtained from the dynamics inside the Goldstein layer. This is also done in Appendix A. The final result is

$$c_4 = \frac{\lambda}{2A_0}\left\{2A_0A_G + e - e^2S + \tfrac{3}{2}S + 2S(I_1 - I_2 - I_3 + I_4) - \frac{4i\pi S}{e^2}\right\}, \tag{3.7}$$

where $S = 6\lambda_4 A_0/\lambda$ and I_1, I_2, I_3, I_4 are definite integrals (constants). From (3.7) the imaginary part of c_4, c_{4i}, is found to be

$$c_{4i} = -\frac{12\lambda_4 \pi}{e^2}. \tag{3.8}$$

Since $\lambda_4 < 0$, $c_{4i} > 0$ and the flow is linearly unstable. The last remark follows from the identification of eigensolutions of the Orr–Sommerfeld equation in the limit of vanishing viscosity, since the Rayleigh equation has eigenvalues which come in complex-conjugate pairs. For a discussion of this point the reader is referred to Lin (1955, chapter 8).

4. Long waves, $\alpha \to 0$

The linear stability of parallel shear flows to long-wavelength perturbations has been the subject of a paper by Drazin & Howard (1966). Attention was focused on jet and shear-layer-type profiles, and the results can be extended to wakes. It was found that the details of the basic velocity profile near the wake centreline are insignificant, and results depend on the undisturbed velocity far away from the centreline.

In this section we consider long-wave inviscid perturbations to the wake, using a different approach from that of Drazin & Howard's as well as appropriate wake profiles. This approach reveals the scalings and structures of the various regions involved as well as their physical effects on the dynamics of the flow. The analysis also motivates the nonlinear long-wave stability analysis reported by us elsewhere. Asymptotic solutions of (2.1) in the limit $\alpha \to 0$ are therefore presented. Thus the waves are long compared with the wake thickness but still short compared with their distance from the trailing edge. The basic flow is $\bar{u}(y)$, where $\bar{u}(\pm\infty) = 1$, $\bar{u}'(0) = 0$.

The boundary condition $\psi'(0) = 0$ is imposed on the perturbation stream function; this means that our study is confined to sinuous velocity modes which are believed to be more unstable than even ones (Drazin & Howard 1962), and are in accord with experimental observations (e.g. the von Kármán vortex street).

The following expansions are appropriate in a region $y = O(1)$ referred to as region I:

$$\psi = \psi_0 + \alpha^{\frac{1}{3}}\psi_1 + \alpha\psi_2 + \alpha^{\frac{3}{3}}\psi_3 + \alpha^2\psi_4 + \ldots, \tag{4.1a}$$

$$c = c_0 + \alpha^{\frac{1}{3}}c_1 + \ldots. \tag{4.1b}$$

The objective is to find the values of c_0, c_1 that are the solution of the eigenvalue problem subject to the relevant boundary conditions. This is done by means of matched asymptotic expansions.

When (4.1 a, b) are substituted into (2.1) and powers of $\alpha^{\frac{1}{3}}$ are equated the following equations are found for the four leading components of ψ:

$$(\bar{u} - c_0)\psi_0'' - \bar{u}''\psi_0 = 0, \tag{4.2a}$$

$$(\bar{u} - c_0)\psi_1'' - \bar{u}''\psi_1 = c_1\psi_0'', \tag{4.2b}$$

$$(\bar{u} - c_0)\psi_2'' - \bar{u}''\psi_2 = c_1\psi_1'' + c_2\Psi_0'', \tag{4.2c}$$

$$(\bar{u}-c_0)\,\psi_3''-\bar{u}''\psi_3 = c_1\psi_2''+c_2\psi_1''+c_3\psi_0'', \tag{4.2d}$$

$$(\bar{u}-c_0)\,\psi_4''-\bar{u}''\psi_4 = c_1\psi_3''+c_2\psi_2''+c_3\psi_1''+c_4\psi_0''+(\bar{u}-c_0)\,\psi_0. \tag{4.2e}$$

The solution of (4.2*a*) that satisfies $\psi_0'(0) = 0$, is the simple displacement solution, $\psi_0 = A_0(\bar{u}-c_0)$, where A_0 is a constant. To satisfy decay at infinity we need $c_0 = 1$, and so $\psi_0 = A_0(\bar{u}-1)$. It can be seen that for small A_0 the total velocity to leading order is $u = \bar{u}(A_0+y)$, which represents a displacement of the basic flow by a small distance A_0. The displacement effect arises from the dynamics inside the Goldstein layer which essentially enables the change in boundary conditions (from no-slip in $x < 0$ to symmetric wake profiles) to be achieved. The solutions of (4.2*b–d*) are

$$\psi_1 = -c_1A_0, \quad \psi_2 = -c_2A_0, \quad \psi_3 = -c_3A_0. \tag{4.3}$$

These are determined by use of the boundary condition at $y = 0$. Strictly, ψ_1, ψ_2, ψ_3 contain additive contributions proportional to $(\bar{u}-1)$ which can be ignored by renormalization of A_0. Equation (4.2*e*), then, has the following general solution that excludes odd contributions:

$$\psi_4 = A_0(\bar{u}-1)\int_0^y \frac{\mathrm{d}y_1}{(\bar{u}-1)^2}\int_\infty^{y_1}(\bar{u}-1)^2\,\mathrm{d}y_2 + d_4(\bar{u}-1)\int_0^y \frac{\mathrm{d}y_1}{(\bar{u}-1)^2} - c_4A_0 + \frac{c_4A_0(\bar{u}-1)}{\bar{u}(0)-1}. \tag{4.4}$$

The undisturbed flow, $\bar{u}(y)$, is assumed to have exponential decay as $|y| \to \infty$; more precisely we assume $\bar{u} \sim 1-Q\,\mathrm{e}^{-\gamma|y|}$ as $|y| \to \infty$ where Q, γ are positive constants. This model of exponential decay at infinity (rather than the full Blasius one which has $\bar{u} \sim 1-(A/|y|)\,\mathrm{e}^{-y^2}$ as $|y| \to \infty$, $A > 0$) has been assumed because analytical progress is simpler with the model and it can be used for clarity since the effect of the actual decay is qualitatively the same. Also, the model analysis can be used to generate ideas and to provide a structure underlying the numerical calculations to follow.

Analytically we find that the expansions (4.1*a*, *b*) break down when $y \sim -(2\gamma)^{-1}\ln\alpha$, owing to the exponential growth of ψ_4 for large y which eventually makes the terms $\alpha^{\frac{3}{2}}\psi_3$ and $\alpha^2\psi_4$ of the same order. A new outer region II must be considered therefore, the solutions of which must match with those of region I. Also, in order to satisfy the boundary conditions at infinity, a third region, III say (essentially a potential flow region), is required. Solution and matching across these regions fixes the value of c_1, which is given below. The details of the asymptotic analysis are given in Appendix B.

The value of c_1 is given by,

$$c_1 = \pm\mathrm{i}\left(\int_0^\infty (\bar{u}-1)^2\,\mathrm{d}y\right)^{\frac{1}{2}}. \tag{4.5}$$

It has been shown, therefore, that long waves are almost neutral and have growth rates of $O(\alpha^{\frac{1}{2}})$ as $\alpha \to 0$ (cf. (4.1*b*), (4.5)) with the leading-order wave speed being equal to the free-stream velocity (in fact equal to $\frac{1}{2}(\bar{u}(\infty)+\bar{u}(-\infty))$ in general). This result is in complete agreement with Drazin & Howard's (1966) treatment of long-wave linear instability in parallel shear flows, but calculated by a more revealing approach. As mentioned earlier it seems that low-frequency/long waves are the relevant disturbances in the nonlinear regime. The asymptotic structures indicated here can, therefore, be used to extend perturbations into the nonlinear regime. This is done in Papageorgiou & Smith (1988).

5. Neutral stability

In the previous sections the stability of the wake to short- and long-wave disturbances was found to yield almost neutral perturbation characteristics with asymptotically small growth rates (cf. (3.5) and (4.5)). Here we consider the possibility of neutral eigensolutions in the near wake. In order to find neutral modes the basic velocity must be considered more closely, of course, and its inflexion points identified. The inflexion points are necessary for the existence of neutral solutions. This is a well-known result in hydrodynamic stability theory and was first analysed by Tollmien (1935); for a description see also Lin (1955) and Drazin & Reid (1981). If the inflexion point occurs at $y = y_c$ then the neutrally stable eigensolution is

$$\psi = \psi_c, \quad \alpha = \alpha_c > 0, \quad c = \bar{u}(y_c) = c_s. \tag{5.1}$$

In the notation of §3, the streamwise velocity u inside the Goldstein layer can be expanded in powers of $\epsilon(\epsilon = x^{\frac{1}{3}} \ll 1)$, as follows:

$$u = \tfrac{1}{3}\epsilon\{f_0(Z) + \epsilon^3 f_3(Z) + O(\epsilon^6)\}.$$

Here $f_0''' + 2f_0 f_0'' - f_0'^2 = 0$ subject to $f_0(0) = f_0''(0) = 0$. Our main concern is with the asymptotic form of f_0 for large Z. Goldstein finds

$$f_0 \sim \tfrac{1}{2}\gamma_0 Z'^2 + \epsilon_0 \exp\left(-\tfrac{1}{3}\gamma_0 Z'^3\{(\gamma_0 Z'^2)^{-2} + \ldots\}\right),$$

where $Z' = Z + \delta_0$ and $\gamma_0, \delta_0, \epsilon_0$ are constants. This flow matches with the Blasius flow as $Z \to \infty$. Owing to the complicated nature of the true Goldstein flow, we consider the following model profile (see earlier comments regarding the choice of a model profile):

$$\bar{u} = \bar{u}(y) \quad (y = O(1)), \quad \bar{u} \sim \lambda y + \lambda_2 y^2 + \ldots \quad \text{as} \quad y \to 0+, \quad (\lambda_2 < 0), \tag{5.2}$$

and for $y = \epsilon Z$, $Z = O(1)$, $\bar{u} = \epsilon F(Z)$ where

$$F(Z) \sim \lambda Z + \gamma e^{-Z} + A_G \quad \text{as} \quad Z \to \infty. \tag{5.3}$$

In (5.3), A_G is a Goldstein displacement constant and γ some positive constant. The position of the inflexion point can be found by combining (5.2), (5.3) and balancing their second derivatives. This yields an inflexion point at $Z = -\ln\epsilon + O(1)$ or $y = \epsilon L + O(\epsilon)$, where $L = -\ln\epsilon \gg 1$. In what follows we describe asymptotic neutral wave solutions valid for all y.

Solutions must be found, and matched with neighbouring regions, in each of the zones I_1, I_2, II, III shown in figure 2. The half-plane $y \geqslant 0$ alone is considered owing to the symmetry of the problem. It can be seen from (5.1) and the calculation of the inflexion point position that the neutral wave speed must have the expansion

$$c = \epsilon L\lambda + \epsilon c_0 + \ldots \quad (= \bar{u}(y_c)). \tag{5.3}$$

An expansion for α follows from a balance of terms in the Rayleigh equation. This gives

$$\alpha = \frac{\alpha_0}{\epsilon L} + \alpha_1 + O(\epsilon L). \tag{5.4}$$

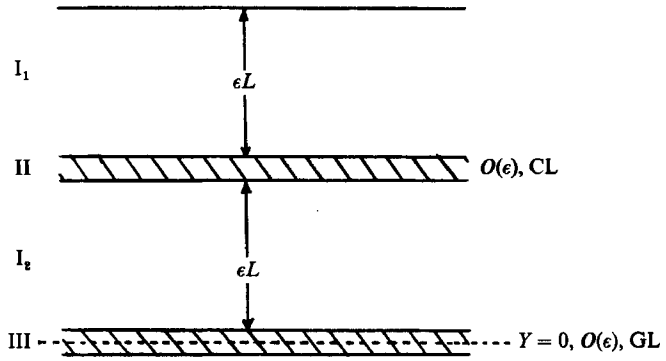

FIGURE 2. The various regions in which neutral waves develop.

With these expansions each of the four regions shown in figure 2, are solved and matched consistently in order to calculate c_1 and α_0 in (5.3) and (5.4) respectively. This is done in Appendix C, and here we give the final results,

$$\alpha = (\epsilon L)^{-1} + \ldots, \quad c = \epsilon L\lambda - \epsilon\lambda \ln\left(\frac{2|\lambda_2|}{\gamma}\right) + \ldots, \tag{5.5}$$

which imply a neutral wave frequency $\beta = \alpha c = \lambda + O(L^{-1})$.

It is interesting to note that the neutral waves have short wavelengths. The question that arises, therefore, is whether these will dominate over the unstable short waves described in §3, and if so over what lengthscales. The results of §3 were based on the ordering $\alpha^{-4} = \epsilon$. Hence, typical wavelengths for short waves are $O(\epsilon^{\frac{1}{3}})$ whereas for neutral waves they are $O(\epsilon L)$. Recall that $\epsilon = x^{\frac{1}{3}}$ and $x \ll 0$. The lengthscales over which short waves are unstable are therefore larger than those over which neutral waves can be found (in fact the lengthscales are $x^{\frac{1}{12}}$ and $-x^{\frac{1}{3}}\ln(x)$ as $x \to 0$). Our results indicate, therefore, that even though neutral waves may be possible in certain regimes, the unstable waves would take over and develop into unstable perturbations.

6. Numerical solutions of the Rayleigh equation

The asymptotic solutions presented in the previous sections do not provide the largest amplification rates. These are achieved when the wavelength or the frequency are order-one parameters, and the problem must be tackled numerically then. Hence we must solve the Rayleigh equation together with the boundary conditions (cf. (2.1)), for general values of the wavenumber or frequency and a prescribed undisturbed velocity profile. This corresponds to an eigenvalue problem for α and c. Results are obtained for two cases. In the first case the eigenvalue problem is solved for real values of α which produce complex eigenvalues c in general; this is the temporal stability of a prescribed basic flow profile. Second, for $\omega = \alpha c$ kept real the corresponding eigenvalues for α and c are complex in general; this corresponds to disturbances growing or decaying with downstream distance and is the spatial stability problem. A combined stability analysis that involves complex frequencies and wavenumbers is in principle possible. It has been observed, however, both experimentally and from numerical calculations (e.g. Mattingly & Criminale 1972) that spatial growth rates describe the stability characteristics very well. Temporal results may be connected via the Gaster group velocity transformation (Gaster 1968)

to yield spatial results in a few limited ranges (see later comments). It should be noted that our asymptotic results of §§3, 4 and 5 are consistent with the comments above, since the growth rates in these analytical regimes are small (in fact asymptotically so) and as a consequence the Gaster transformation is valid.

As mentioned in the previous sections, the most unstable modes are observed to be the sinuous ones, i.e. those having stream functions that are even about the wake centreline. This limits the numerical range of integration to the upper half-plane and thus halves computational times. The range of dependence is taken to be $0 \leqslant y \leqslant y_\infty$, where y_∞ is a suitably large number. The unperturbed flow for the different calculations will be discussed in detail later on in this section.

The object is to solve the Rayleigh equation (2.1), and in particular to find the eigenvalues for the appropriate boundary conditions. The range $(0, y_\infty)$ is divided into J equal subintervals of length h. The velocity profile is now approximated by a piecewise linear distribution in each of the intervals, a fact that simplifies the Rayleigh equation in each interval considerably since the $\bar{u}''$ term is zero. Hence if the discretization points are $y_j : j = 1 \to J+1$ with $y_1 = 0$, $y_{j+1} = y_\infty$, then the stream function in the interval (y_j, y_{j+1}), denoted by $\psi^{(j)}$, satisfies

$$\frac{\mathrm{d}^2}{\mathrm{d}y^2}\psi^{(j)} - \alpha^2\psi^{(j)} = 0, \quad j = 1, \ldots, J.$$

The solutions are

$$\psi^{(j)} = A_j \mathrm{e}^{\alpha(y-y_j)} + B_j \mathrm{e}^{-\alpha(y-y_j)}, \tag{6.1}$$

where A_j, B_j are constants to be determined. These are two equations that connect the values of A_j, B_j in neighbouring intervals. These come from continuity of mass flux and pressure across points of discontinuity ($\bar{u}'$ is discontinuous at $y = y_j$), and are

$$(A_j + B_j)/(\bar{u}_j - c) = (A_{j-1}\mathrm{e}^{\alpha h} + B_{j-1}\mathrm{e}^{-\alpha h})/(\bar{u}_j - c), \tag{6.2a}$$

$$\alpha(\bar{u}_j - c)(A_j - B_j) - \bar{u}'_{j+}(A_j + B_j) = \alpha(\bar{u}_j - c)(A_{j-1}\mathrm{e}^{\alpha h} - B_{j-1}\mathrm{e}^{-\alpha h}) - \bar{u}_{j-}(A_{j-1}\mathrm{e}^{\alpha h} + B_{j-1}\mathrm{e}^{-\alpha h}), \tag{6.2b}$$

respectively, where $\bar{u}_j = \bar{u}(y = y_j)$, $\bar{u}'_{j\pm}$ is the velocity gradient in the interval above and below $y = y_j$. The system (5.2a, b) together with the boundary conditions of decay at infinity and evenness of ψ at the origin, fix the eigenvalue problem for α and c. The condition at infinity ($y = y_{J+1}$) is

$$A_J \mathrm{e}^{\alpha h} + B_J \mathrm{e}^{-\alpha h} = 0.$$

The boundary condition at the origin requires a little more care, however, depending on the underlying basic flow. In most of the calculations presented here the basic flow satisfies $\bar{u}'(y = 0) = 0$ (proper wake profiles), but for completeness we also consider a double Blasius distribution which gives the distribution in the limit $x \to 0$. For wake profiles in $x > 0$ the condition at $y = 0$ becomes

$$\psi(y = 0) = \text{constant},$$

whereas for the double Blasius form holding at the outset $x = 0$ we obtain

$$A_1 = \tfrac{1}{2}q\left(1 - \frac{\lambda}{\alpha c}\right), \quad B_1 = \tfrac{1}{2}q\left(1 + \frac{\lambda}{\alpha c}\right),$$

where λ is the slope of the Blasius distribution at the origin, and $\psi(0+) = \psi(0-) = q$. The difference equations (6.2a, b) can now be used to obtain the values of the A_j, B_j. Numerically this is done by Newton iteration since the system is nonlinear with

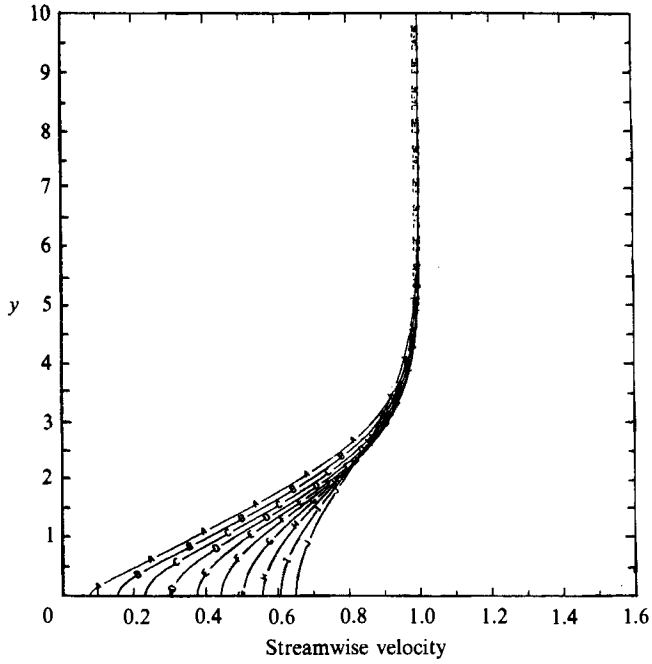

FIGURE 3. Unperturbed velocity profiles at different streamwise positions. The flow is symmetric about $y = 0$. Profiles are shown, from left to right, at $\xi = 0.1$, 0.2, 0.3, 0.4, 0.5, 0.6, 0.7, 0.8, 0.9 and 1.0.

respect to the A_j, B_j and c. In other words initial guesses are made for the unknowns and linear increments are calculated by solution of a system of linear equations. The system is solved by matrix inversion. Eigenvalues can be obtained in this way for both temporal and spatial stability. The numerical parameters J, h and y_∞ are varied to establish numerical convergence of the method. Before a description of the results we present some details on the basic flow profiles used in the computations.

The unperturbed flow in the wake considered here is a solution of the boundary-layer equations subject to wake boundary conditions. The governing equations are, therefore, in the usual boundary-layer notation

$$UU_x + VU_y = U_{yy},$$

$$U_x + V_y = 0,$$

$$U_y(x, y = 0) = 0, \quad V(x, y = 0) = 0, \quad U(x, \infty) = 0.$$

The starting condition at $x = 0$ is

$$U(x = 0+, y) = U_B(y),$$

where $U_B(y)$ is the Blasius velocity distribution. This is required in the matching of the wake to the trailing-edge flow.

The asymptotic results of Goldstein, already discussed in §3, can be utilized in a way that captures the delicate physical mechanisms in the vicinity of the trailing edge and the wake centreline and so enable the efficient and accurate computation of the flow. Such methods have been developed, for different boundary-layer problems, by Keller & Cebeci (1971) and Smith (1974) for example. Calculations of symmetric wakes employing adaptive-grid methods have been carried out by Cebeci *et al.* (1979), and we make a comparison of our results with theirs.

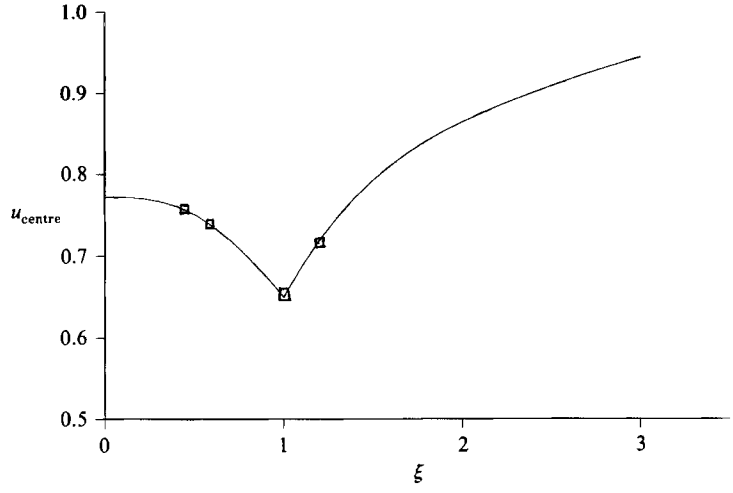

FIGURE 4. Streamwise variation of centreline velocity in the unperturbed wake. From $\xi = 0$ to $\xi = 1$ the value of u_{centre}/ξ is shown. For $\xi \geqslant 1 u_{centre}$ is plotted. □, indicates results from the calculations of Cebeci *et al.* (1979).

Some of the calculations for the streamwise component of the flow U, at increasing downstream stations, are shown in figure 3. The transition from Blasius flow to a wake flow is evident and the downstream-infinity value for U is unity. In figure 4 the streamwise variation of centreline velocity obtained from our calculations is shown. The results of Goldstein and Cebeci *et al.* are indicated for comparison and agreement is excellent. In what follows, the stability characteristics of the flow at different streamwise positions are computed. The computations take into account the non-parallel nature of the flow by a quasi-parallel assumption, and use the proper wake profiles as given by the governing equations. Since linear stability is considered here, profiles lying in a region $0 < x < x_0$ may be used, where x_0 is the extent of the linear regime. The value of x_0 has been determined experimentally by Sato & Kuriki (1961) and for large Reynolds numbers it is approximately one fifth of the plate's length; in other words about 0.2 in non-dimensional terms.

7. Results and discussion

First we show some results for the double Blasius distribution holding right at the start of the wake. The aim is to provide a comparison between numerical and asymptotic solutions, and in particular to verify the range of validity of our asymptotic expansions. Temporal calculations are therefore performed. Figures 5(*a*) and 5(*b*) show a comparison of numerical and asymptotic results in the cases $\alpha \to \infty$, $\alpha \to 0$; in the former case the distribution of c_r against α is shown and in the latter that of c_i against α. The leading-order asymptotic results of §§3, 4 are used and agreement is seem to be fairly good. In the eigenvalue calculations of long waves, it becomes both expensive and inaccurate to compute solutions for α too small ($\alpha \sim 10^{-3}$ say), because a grid of extent $O(\alpha^{-1})$ is required in order to capture the physics of the problem. In addition to this, terms of $O(\alpha)$ are ignored and so it is not surprising that the agreement between asymptotic and numerical results in the long-wave case is not as striking as the short-wave results where the error term is $O(\alpha^{-3})$, $\alpha \gg 1$. In figure 6 the temporal growth rate and wave speed are depicted for the

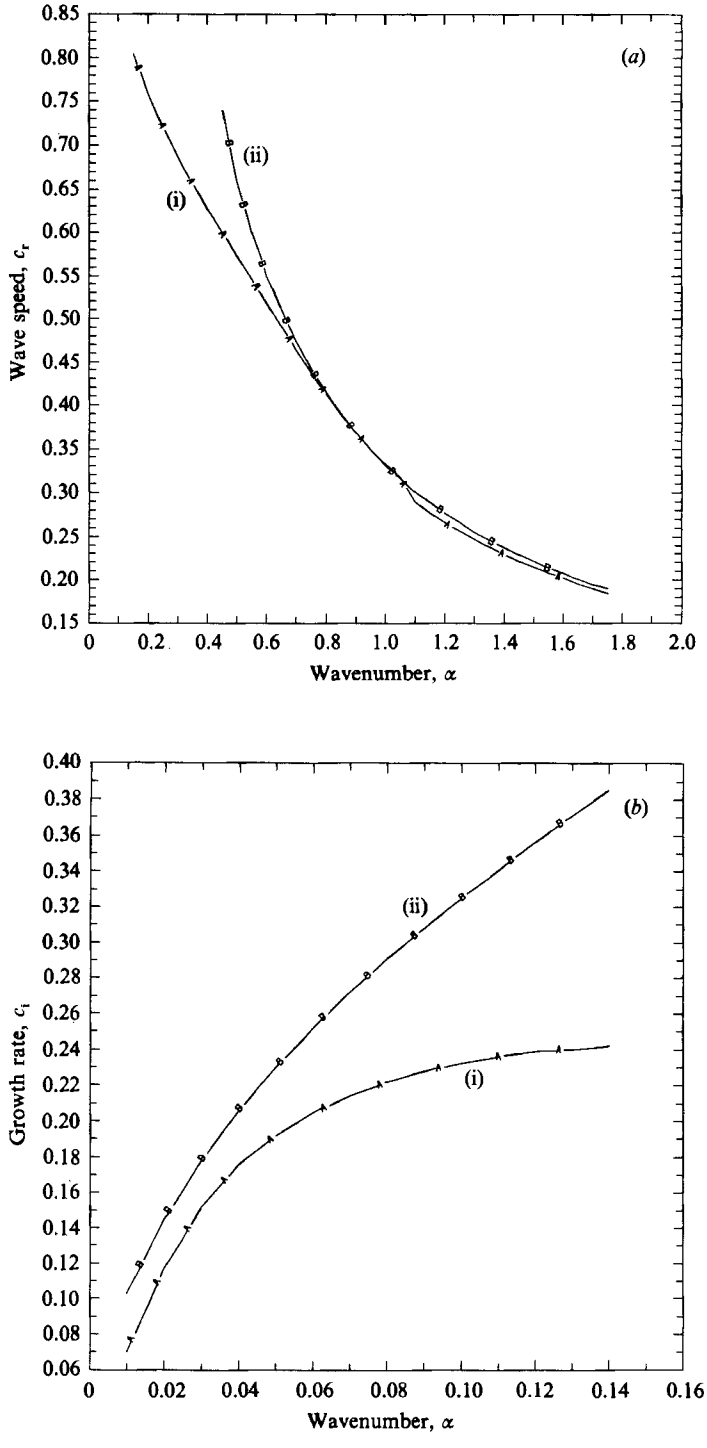

FIGURE 5. Comparison between asymptotic results and numerical calculations. (*a*) Short waves. Variation of Re (*c*) with wavenumer. (*b*) Long waves. Variation of Im (*c*) with wavenumber. Curve (i) asymptotic, curve (ii) numerical.

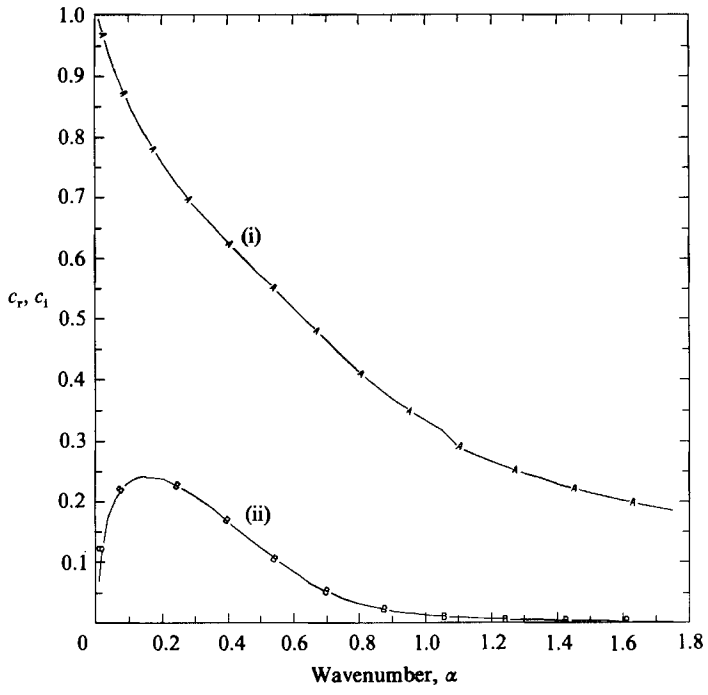

FIGURE 6. Temporal stability of the double Blasius distribution. Curve (i) variation of c_r with α. Curve (ii) variation of c_i with α.

double Blasius profile, for a full range of wavenumbers. The maximum growth rate is seen to be attained at the long-wavelength end of the neutral curve.

As mentioned earlier, spatial stability calculations are more relevant physically than temporal ones, unless the temporal growth rates are small enough that the Gaster transformation may be used to connect the two situations. As this is not the case in the near wake where the disturbances first experience substantial growth, we choose to concentrate on spatial stability. Figure 7 shows a collection of curves at various streamwise locations. The streamwise coordinate indicated is ξ and is given by $\xi = x^{\frac{1}{3}}$, where x is non-dimensional distance from the trailing edge. The curves depict the variation of spatial growth rate $(-\alpha_i)$ as a function of frequency ω. The smallest value of ξ at which eigenvalues were computed is 0.02. This corresponds to a distance 0.000008 from the trailing edge. The maximum growth rate is seen to decrease with streamwise distance and is attained at larger values of the frequency. As a consequence the unstable band of frequencies broadens but the maximum growth rate decreases. Our computations do not seem to indicate a streamwise position where the spatial growth rate is a maximum, but instead such a point moves towards the trailing edge.

In order to compare with experiments and previous calculations, the stability of the basic flow at the position $x = 0.1$ is computed in detail. This station is chosen to coincide with the experimental station of Sato & Kuriki (referred to as S & K). A considerable number of theoretical results have been predicted by Mattingly & Criminale (referred to as M & C), based on empirical basic flow profiles. The profiles used by them, however, seem to deviate from the appropriate theoretical ones of Goldstein and of the present computations (for example, at $x = 0.5$ the centreline velocity of M & C is about half the theoretical one; see figure 4 of M & C). S & K also

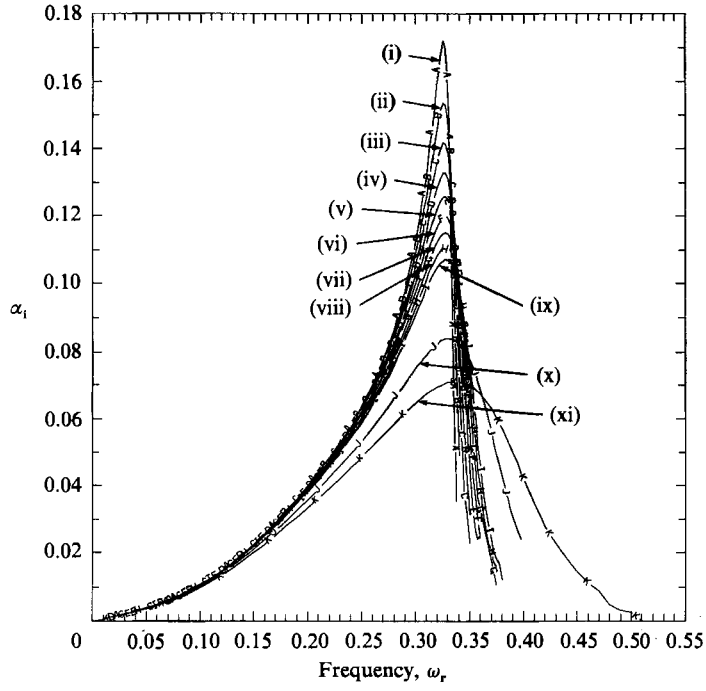

FIGURE 7. Spatial stability of proper wake profiles at various streamwise positions. The graphs show the spatial growth rate $-\alpha_i$ as a function of the frequency ω. Curve (i) is at $\xi = 0.02$, (ii) 0.03, (iii) 0.04, (iv) 0.05, (v) 0.06, (vi) 0.07, (vii) 0.08, (viii) 0.09, (ix) 0.1, (x) 0.2, (xi) 0.3.

fit a profile to the observed flow and calculate its stability via the Rayleigh equation. This is done for temporally growing waves which are then compared to experiments by the group velocity transformation, which in our view represents an irrational step. In figure 8 we show our spatial calculations at the non-dimensional station $x = 0.1$ (S & K experiment was at $x^* = 30$ mm for a plate of length 300 mm), and compare with S & K theory and experiment. The graph shows the spatial growth rate $(-\alpha_i)$ as a function of the frequency ω. Agreement is quantitatively not as good as would be desired but given the fact that the theory is linear and parallel (at a frozen x-station) agreement is qualitatively good. Figure 9 shows the variation of c_r, α_r with frequency as found in our calculations and by S & K. Another comparison of our theoretical predications and the experimental results of S & K is shown in figure 10. Here the streamwise growth in amplitude of the spectral components of the disturbances is shown. These are calculated as follows. For the appropriate non-dimensional forcing frequency of an experiment, eigenvalues of the Rayleigh equation are calculated at a given x-station. The amplitude of the disturbance at a given position is proportional to $\exp(|\alpha_i| R_e^{\frac{1}{2}} X)$. The position X is now increased and the growth factor is noted. For different streamwise positions, therefore, the lines of growth can be calculated by the use of correct profiles in the Rayleigh equations. These are the lines labelled * and are compared to those of S & K.

It can be seen from the results in figures 6–10, that agreement between the linear theory and the experimental findings is quite good. At first sight it might seem that the temporal-stability approach together with the Gaster transformation provides a good description of the instability but although the agreement produced is qualitatively good for distances far enough from the trailing edge, it is not so closer

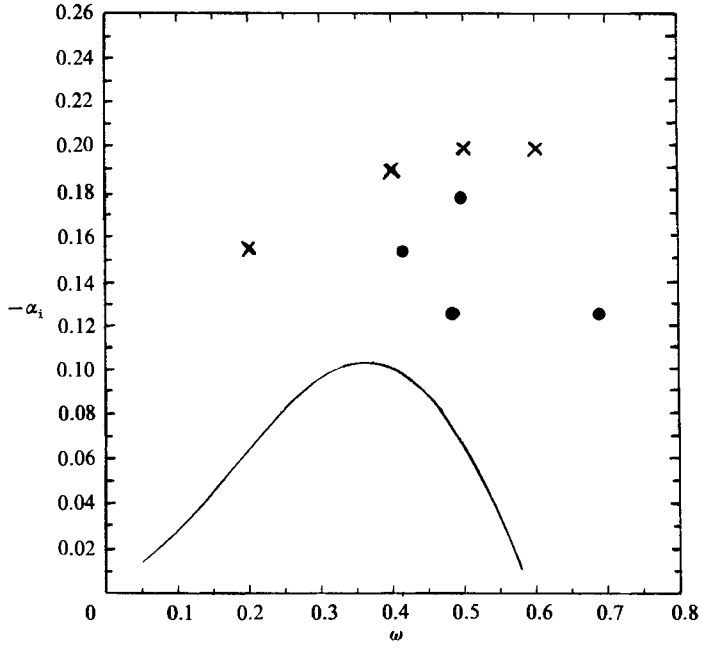

FIGURE 8. Spatial stability of the wake at $x = 0.1$ ($\xi = 0.465$). Variation of $-\alpha_i$ with ω. Curve, present numerical calculations; ×, Sato & Kuriki temporal calculations together with the group velocity transformation; ●, Sato & Kuriki experiments.

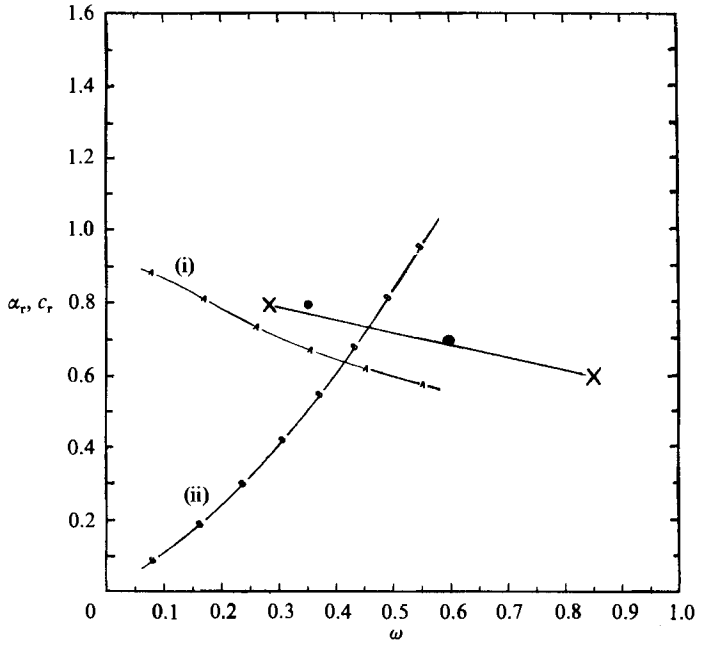

FIGURE 9. Spatial stability of the wake at $x = 0.1$ ($\xi = 0.465$). Curve (i) variation of α_r with ω; curve (ii) variation of c_r with ω; ×, Sato & Kuriki temporal calculations; ●, experiments.

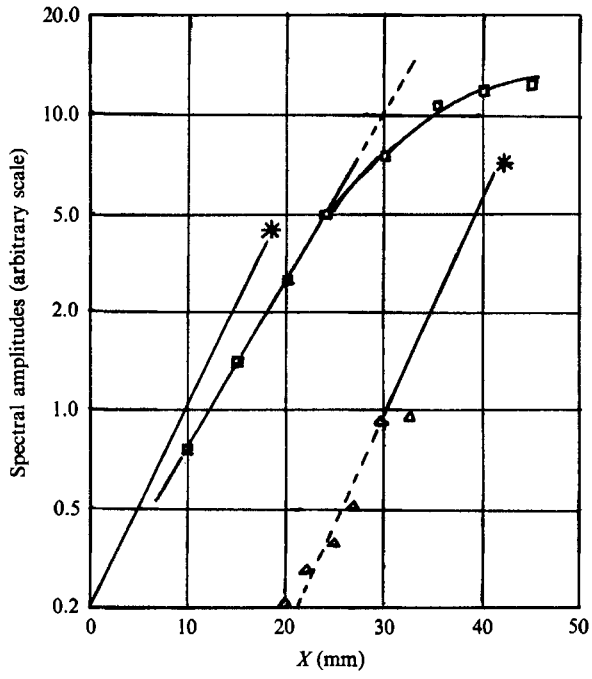

FIGURE 10. Lines of growth of the disturbances. Comparison between theory and experiment. Sato & Kuriki experiments: □, excitation 650 c/s; △, excitation 850 c/s; *, present theory.

to the trailing edge where the spatial growth rates are no longer 'small'. Hence the full spatial-stability analysis does seem necessary.

Our neutral stability results can also be compared with the experimental results of S & K. They measured velocity fluctuations in the wake using hot-wire anemometry and presented oscillographic records of the u-fluctuations (see figure 5 in that paper). One of the traces ($x = 30$ mm, $y = 1$ mm) exhibits neutral behaviour with frequency ~ 800, for a free-stream velocity $u_\infty^* = 10\ \mathrm{ms}^{-1}$. This implies that the dimensional frequency of oscillation, ω^* say, is $2\pi \times 800 \sim 5024$ Hz. The Reynolds number for the experimental flow is $R_e \sim 2.3 \times 10^5$. If we denote the plate length by l^*, then $l^* = 0.3$ m and the boundary-layer thickness $l^* R_e^{-\frac{1}{2}}$ is approximately 1 mm. The dimensional form of the time is $t^* = l^* R_e^{-\frac{1}{2}} T / u_\infty^*$, where T is the non-dimensional time used in the linearized Euler equations when the Rayleigh equation was derived. Thus linear waves have time dependence of the form

$$\exp(\mathrm{i}\beta T) = \exp\left(\mathrm{i}\beta \frac{u_\infty^*}{l^*} R_e^{\frac{1}{2}} t^*\right) = \exp(\mathrm{i}\omega^* t^*).$$

Hence our theoretical result predicts a frequency $\omega^* = \beta(u_\infty^*/l^*) R_e^{\frac{1}{2}}$, where $\beta = \lambda(= 0.332\ldots)$ from (5.5); notice that β has this value, to leading order, in the case of short waves also (cf. (3.5)) which are almost neutral anyway. This value works out to be ≈ 5200 Hz, in quite good agreement with the above experimental value of 5024 Hz (relative error $\approx 5\%$).

The numerical calculations based on the Rayleigh equation and proper wake profiles provide fair agreement with experimental data, then. Our results indicate further that a spatial stability analysis is appropriate here, as is also the case for the related problems of jet and free shear-layer stability.

With the linear stability results and structures available now for the asymptotically correct wake profiles, it is possible to proceed rationally into the nonlinear regime. Perhaps the most interesting case indicated by experiments, and on theoretical grounds, concerns the nonlinear evolution of long waves and this is being addressed in subsequent work by the authors.

We would like to thank the referees for some useful and interesting comments regarding an earlier version of this work. Professor Andreas Acrivos of City College of New York is also thanked for some fruitful discussions. One of us (D.T.P.) acknowledges the receipt of a support grant from the SERC, UK, during part of this research.

Appendix A

Let $\psi_3^{(1)}, \psi_3^{(2)}, \psi_3^{(3)}, \psi_3^{(4)}$ represent solutions in regions (1), (2), (3) and (4) respectively; then the governing equations are

$$\frac{\mathrm{d}^2\psi_3^{(i)}}{\mathrm{d}Y^2} - \psi_3^{(i)} = \frac{12\lambda_4 A_0 Y^2 \mathrm{e}^{-Y}}{\lambda(Y-1)}, \quad i = 1, 2, \tag{A 1a, b}$$

$$\frac{\mathrm{d}^2\psi_3^{(i)}}{\mathrm{d}Y^2} - \psi_3^{(i)} = -\frac{12\lambda_4 A_0 Y^2 \mathrm{e}^{Y}}{\lambda(Y+1)}, \quad i = 3, 4. \tag{A 1c, d}$$

These can be solved, subject to the boundary condition that the disturbance vanishes at $y = \pm\infty$ to give

$$\psi_3^{(1)} = \mathrm{e}^{-Y}\left[B_3^{(1)} - \frac{6\lambda_4 A^0}{\lambda}\{\tfrac{1}{2}Y^2 + Y + \ln(Y-1)\}\right] + \mathrm{e}^{Y}\frac{6\lambda_4 A_0}{\lambda}\int_{\infty}^{Y} Y^2 \frac{\mathrm{e}^{-2Y}}{(Y-1)}\mathrm{d}Y, \tag{A 2a}$$

$$\psi_3^{(2)} = \mathrm{e}^{-Y}\left[B_3^{(2)} - \frac{6\lambda_4 A^0}{\lambda}\{\tfrac{1}{2}Y^2 + Y + \ln(1-Y)\}\right] + \mathrm{e}^{Y}\left[A_3^{(2)} + \frac{6\lambda_4 A_0}{\lambda}\int_{0}^{Y} Y^2 \frac{\mathrm{e}^{-2Y}}{(Y-1)}\mathrm{d}Y\right], \tag{A 2b}$$

$$\psi_3^{(3)} = \mathrm{e}^{Y}\left[B_3^{(3)} - \frac{6\lambda_4 A^0}{\lambda}\{\tfrac{1}{2}Y^2 + Y + \ln(1+Y)\}\right] + \mathrm{e}^{-Y}\left[A_3^{(3)} + \frac{6\lambda_4 A_0}{\lambda}\int_{0}^{Y} \frac{Y^2 \mathrm{e}^{2Y}}{(1+Y)}\mathrm{d}y\right], \tag{A 2c}$$

$$\psi_3^{(4)} = \mathrm{e}^{Y}\left[B_3^{(4)} - \frac{6\lambda_4 A_0}{\lambda}\{\tfrac{1}{2}Y^2 + Y + \ln|1+Y|\}\right] + \mathrm{e}^{-Y}\frac{6\lambda_4 A_0}{\lambda}\int_{-\infty}^{Y} \frac{Y^2 \mathrm{e}^{2Y}}{(1+Y)}\mathrm{d}Y, \tag{A 2d}$$

The six constants $B_3^{(1)}, B_3^{(2)}, B_3^{(3)}, B_3^{(4)}, A_3^{(2)}, A_3^{(3)}$ are determined below, from matching.

The Goldstein layer (GL) has thickness $\epsilon = x^{\frac{1}{8}} \leqslant 1$, and the local variable Z is introduced, defined by $y = \epsilon Z$. Hence the solution for the stream function inside the Goldstein layer as $Z \to \pm\infty$ must match with $\psi_3^{(2)}, \psi_3^{(3)}$ as $Y \to 0\pm$ respectively. The solutions inside the Goldstein layer expand as follows:

$$\psi_{\mathrm{GL}} = \Psi_0 + \epsilon\alpha\Psi_1 + \epsilon^2\alpha^2\Psi_2 + \ldots, \quad c = \alpha^{-1}c_1 + \epsilon c_4 + \alpha\epsilon^2 c_7 + \ldots. \tag{A 3a, b}$$

The basic flow is that given by Goldstein (1930),

$$\bar{u} = \epsilon F(Z) + \epsilon^4 F_{\mathrm{c}}(Z) + O(\epsilon^7), \quad F(Z) \sim \pm\lambda(Z + A_{\mathrm{G}}), \tag{A 3c}$$

$$F_{\mathrm{c}}(Z) \sim \lambda_4 Z^4 \quad \text{as} \quad Z \to \pm\infty,$$

where A_{G} is a constant, the Goldstein displacement thickness. The forms of the expansions above follow from matching requirements with the outer regions, but since there is an order-one displacement in the expansion for ψ_3 the special limit $\epsilon\alpha = q\alpha^{-3}$ must be chosen for ϵ. With this limit, it is seen that the expansion for the

wave speed is the same as that outside the Goldstein layer if $q = O(1)$. As a referee points out, however, the validity of the expansion can be improved by a double expansion in α^{-1} and $\epsilon\alpha$. In this case the restriction is $\epsilon\alpha \ll 1$. We do not give the details of this here (the analysis is similar to that presented below), but we have found that the final result, namely (3.7) and (3.8), remain unaltered. Matching leading-order terms of the stream function outside and inside the Goldstein layer respectively gives $\Psi_0 = A_0$. Substituting (A 3*a–c*) into the Rayleigh equation yields the following expressions for the Ψ_1 and Ψ_2 (primes denote Z-derivatives);

$$\Psi_1 = -\frac{A_0}{\lambda}F(Z) + \frac{E_1 Z}{\lambda} + \frac{H_1}{\lambda}, \tag{A 4a}$$

$$\Psi_2' = \left(\frac{A_0 c_4}{\lambda^2} - \frac{H_1}{\lambda^2}\right)F' + A_0 Z - \frac{E_1}{\lambda^2}(ZF' - F) + E_2, \tag{A 4b}$$

where E_1, E_2 and H_1 are constants to be determined.

There is a jump in the slope of the $O(\alpha^{-3})$-outer solution, $\mathrm{d}\psi_3/\mathrm{d}Y$, across $Y = 0$. This can be equated, from matching, with the slope of Ψ_2 from the Goldstein layer solution. The relation obtained is

$$\left[\frac{\mathrm{d}\psi_3}{\mathrm{d}Y}\right]_{0-}^{0+} = \left[\frac{\mathrm{d}\Psi_2}{\mathrm{d}Z}\right]_{-\infty}^{\infty} = 2\lambda\left(\frac{c_4 A_0}{\lambda^2} - \frac{H_1}{\lambda^2}\right) + \frac{2E_1 A_G}{\lambda}. \tag{A 5}$$

The constants E_1, E_2, H_1 can be found by matching the Goldstein solution as $|Z| \to \infty$ with the outer solution as $Y \to 0\pm$ respectively. Hence, $O(\epsilon\alpha)$-terms (i.e. terms involving $\psi_3^{(2)}$ and ψ_1 from the outer solution) give the matching requirement

$$B_3^{(2)} + A_3^{(2)} = \frac{1}{\lambda}(H_1 - \lambda A_0 A_G) = A_3^{(3)} + B_3^{(3)}, \quad E_1 = 0. \tag{A 6}$$

If the jump in $\mathrm{d}\psi_3/\mathrm{d}Y$ is now calculated from the outer solution and the result equated to the jump from the inner solution given by (A 5), the following equation results:

$$(A_3^{(2)} - B_3^{(2)}) + (A_3^{(3)} - B_3^{(3)}) = 2\lambda\left(\frac{c_4 A_0}{\lambda^2} - \frac{H_1}{\lambda^2}\right). \tag{A 7}$$

Substitution for $A_3^{(2,3)}, B_3^{(2,3)}$ into (A 6) and elimination of H_1 gives a value for c_4:

$$c_4 = \frac{\lambda}{2A_0}\left\{2A_0 A_G + e - e^2 S + \tfrac{3}{2}S + 2S(I_1 - I_2 - I_3 + I_4) - \frac{4\mathrm{i}\pi S}{e^2}\right\}$$

where $S = 6\lambda_4 A_0/\lambda$ and I_1, I_2, I_3, I_4 are definite integrals (constants).

Appendix B

The expansion for ψ in region II ($y_{II} = -(1/2\gamma)\ln\alpha + \bar{y}\,(-\infty \leqslant \bar{y} \leqslant \infty)$) is

$$\psi_{II} = \alpha^{\frac{1}{2}}\tilde{\psi}_1 + \alpha\tilde{\psi}_2 + \alpha^{\frac{3}{2}}\tilde{\psi}_3 + \ldots + \alpha^{\frac{5}{2}}\ln\alpha(\hat{\psi}_1 + \alpha^{\frac{1}{2}}\hat{\psi}_2 + \ldots) + \text{h.o.t.}, \tag{B 1}$$

where h.o.t. denotes higher-order terms, and that for the wave speed is the same as before, cf. (4.1*b*). The correct behaviour that matches (B 1) as $\bar{y} \to -\infty$ with the solutions in region I is

$$\left.\begin{aligned} \tilde{\psi}_1 &\sim -A_0 Q\,\mathrm{e}^{-\gamma\bar{y}} - A_0 c_1, \quad \tilde{\psi}_2 \sim -A_0 c_2, \\ \tilde{\psi}_3 &\sim A_0 c_3 - \frac{d_4}{2\gamma Q}\mathrm{e}^{-\gamma\bar{y}}, \quad \hat{\psi}_1 \sim -\frac{A_0 Q}{2\gamma}\mathrm{e}^{-\gamma\bar{y}} \ldots. \end{aligned}\right\} \tag{B 2}$$

The equations satisfied by $\tilde{\psi}_1, \tilde{\psi}_2, \tilde{\psi}_3, \hat{\psi}_1$, together with their general solutions are

$$(-Q\,\mathrm{e}^{-\gamma\bar{y}}-c_1)\,\tilde{\psi}_1''+Q\gamma^2\,\mathrm{e}^{-\gamma\bar{y}}\,\tilde{\psi}_1=0, \quad \tilde{\psi}_1=A_0(-Q\,\mathrm{e}^{-\gamma\bar{y}}-c_1), \tag{B 3a}$$

$$(-Q\,\mathrm{e}^{-\gamma\bar{y}}-c_1)\,\tilde{\psi}_2''+Q\gamma^2\,\mathrm{e}^{-\gamma\bar{y}}\,\tilde{\psi}_2=c_2\tilde{\psi}_1'', \quad \tilde{\psi}_2=-A_0c_2, \tag{B 3b}$$

$$(-Q\,\mathrm{e}^{-\gamma\bar{y}}-c_1)\,\tilde{\psi}_3''+Q\gamma^2\,\mathrm{e}^{-\gamma\bar{y}}\,\tilde{\psi}_3=c_2\tilde{\psi}_2''+c_3\tilde{\psi}_1'', \tag{B 3c}$$

$$\tilde{\psi}_3=e_3(-Q\,\mathrm{e}^{-\gamma\bar{y}}-c_1)\int^{\bar{y}}\frac{\mathrm{d}\bar{y}}{(Q\,\mathrm{e}^{-\gamma\bar{y}}+c_1)^2}+c_3A_0\gamma Q(-Q\,\mathrm{e}^{-\gamma\bar{y}}-c_1)\int^{\bar{y}}\frac{\mathrm{e}^{-\gamma\bar{y}}\,\mathrm{d}\bar{y}}{(Q\,\mathrm{e}^{-\gamma\bar{y}}+c_1)^2},$$

$$(-Q\,\mathrm{e}^{-\gamma\bar{y}}-c_1)\,\hat{\psi}_1''+Q\gamma^2\,\mathrm{e}^{-\gamma\bar{y}}\,\hat{\psi}_1=0, \quad \hat{\psi}_1=(-Q\,\mathrm{e}^{-\gamma\bar{y}}-c_1)\frac{A_0}{2\gamma}. \tag{B 3d}$$

The solution $\tilde{\psi}_3$ matches with that in region I (as $\bar{y}\to-\infty$, $y\to\infty$) if

$$e_3=d_4. \tag{B 4}$$

As $\bar{y}\to\infty$, $\tilde{\psi}_1, \tilde{\psi}_2$ and $\hat{\psi}_1$ tend to constants whereas $\tilde{\psi}_3$ behaves according to

$$\tilde{\psi}_3''-\frac{e_3\bar{y}}{c_1}-\frac{e_3Q}{c_2^2}\bar{y}\,\mathrm{e}^{-\gamma\bar{y}}+\left(\frac{c_3A_0Q}{c_1}-\frac{2e_3Q}{\gamma c_1^2}\right)\mathrm{e}^{-\gamma\bar{y}}+O(\mathrm{e}^{-2\gamma\bar{y}}). \tag{B 5}$$

An outer region, III say, given by $y_{\mathrm{III}}=\alpha^{-1}Y$ $(0\leqslant Y\leqslant\infty)$ is needed to complete the matching. The expansion is

$$\psi_{\mathrm{III}}=\alpha^{\frac{1}{2}}\Psi_0+\alpha\Psi_1+\alpha^{\frac{3}{2}}\Psi_2+\ldots+\mathrm{e}^{-\alpha^{-1}\gamma Y}(\Psi_0+\alpha^{\frac{1}{2}}\tilde{\Psi}_1+\ldots)+\text{h.o.t.} \tag{B 6}$$

The term h.o.t. includes terms of orders $(\alpha\ln\alpha)\,\mathrm{e}^{-\alpha^{-1}\gamma Y}$, $\alpha^{\frac{3}{2}}\ln\alpha$, $\alpha^{\frac{1}{2}}\mathrm{e}^{-2\alpha^{-1}\gamma Y}$. The matching requirement for Ψ_0 is

$$\Psi_0\sim-A_0c_1-\frac{e_3}{c_1}Y \quad \text{as} \quad Y\to0+. \tag{B 7}$$

The Rayleigh equation provides the solution for Ψ_0; using (B 7) also, we find

$$\Psi_0=K\,\mathrm{e}^{-Y}, \quad K=-A_0c_1=\frac{e_3}{c_1}. \tag{B 8}$$

It follows from (B 8) and (B 4) that

$$e_3=d_4=-A_0c_1^2. \tag{B 9}$$

The value of d_4 can also be calculated from the boundary condition $\psi_4'(0)=0$. Hence, it is found from (4.4) that

$$d_4=A_0\int_0^\infty(\bar{u}-1)^2\,\mathrm{d}y,$$

which in conjunction with (B 9) yields

$$c_1=\pm\mathrm{i}\left(\int_0^\infty(\bar{u}-1)^2\,\mathrm{d}y\right)^{\frac{1}{2}}.$$

Appendix C

Consider first the solution in I_1. Here $y=\epsilon LY$ where $Y=O(1)$ and $1<Y\leqslant\infty$; the expansions are

$$\psi_{\mathrm{I}_1}=\Psi_0+\epsilon L\Psi_1+O(\epsilon^2L^2), \tag{C 1a}$$

$$\bar{u}_{\mathrm{I}_1}=\epsilon LY+\epsilon^2L^2\lambda_2\,Y^2\ldots+\epsilon\gamma\,\mathrm{e}^{-LY}+\ldots. \tag{C 1b}$$

These expansions are in powers of ϵL except for the term $\epsilon\,\mathrm{e}^{-LY} = \epsilon^{Y+1}$ that can complicate matters. When balances between terms are set up, however, the importance of such ϵ^{Y+1} terms can be accounted for correctly. In region I_1, at $O(\epsilon^{-1}L^{-1})$ the Rayleigh equation yields

$$\lambda(Y-1)\,(\Psi_0''-\alpha_0^2\,\Psi_0) = 0. \tag{C 2}$$

To obtain this, the term of order ϵ^{Y-1} is assumed to be small compared with $\epsilon^{-1}L^{-1}$. Since $Y > 0$ this holds in both I_1 and I_2 and the governing equation, at leading order, is the same ((C 2)) in both regions. Next, at $O(1)$, we obtain

$$\Psi_1''-\alpha_0^2\,\Psi_1 = \frac{2\lambda_2\,\Psi_0}{\lambda(Y-1)}+2\alpha_0\alpha_1\,\Psi_0. \tag{C 3}$$

This is valid as long as $\epsilon^{Y-1} \ll 1$ which holds in I_1, but not in I_2. Hence the leading-order solutions in I_1 are

$$\Psi_0 = A_0\,\mathrm{e}^{-\alpha_0 Y}, \tag{C 4a}$$

$$\Psi_1 = B_1\,\mathrm{e}^{-\alpha_0 Y}+\frac{\lambda_2 A_0}{\alpha_0\lambda}\mathrm{e}^{\alpha_0 Y}\int_\infty^Y\frac{\mathrm{e}^{-2\alpha_0 Y}\,\mathrm{d}Y}{(Y-1)} -\frac{\gamma_2 A_0\,\mathrm{e}^{-\alpha_0 Y}}{\alpha_0\lambda}\left\{\mathrm{e}^{2\alpha_0}\int_\infty^1\frac{\mathrm{e}^{-2\alpha_0 Y}\,\mathrm{d}Y}{(Y-1)}+\int_1^Y\frac{\mathrm{d}Y_1}{(Y_1-1)}-\alpha_1 A_0\,Y\,\mathrm{e}^{-\alpha_0 Y}\right\}. \tag{C 4b}$$

It can be shown that as $Y\to 1+$, $Y-1 \ll 1$,

$$\Psi_1 \sim D_0+(Y-1)\,D_1+(Y-1)\ln(Y-1)\,D_2+O[(Y-1)^2\ln(Y-1)], \tag{C 5}$$

where D_0, D_1, D_2 are constants and (C 5) can be used to continue the solution into region II.

In region II new coordinates are introduced by $y = \epsilon L+\epsilon z$, $-\infty \leqslant z \ll \infty$; since $Y-1 = z/L$ the following series is implied in II;

$$\Psi_{\mathrm{II}} = \psi_0+L^{-1}\psi_1+L^{-2}\psi_2+\ldots+\epsilon L(\tilde{\psi}_0+L^{-1}\tilde{\psi}_1+\ldots)+\epsilon\ln L(\hat{\psi}_0+L^{-1}\hat{\psi}_1+\ldots)+\text{h.o.t.} \tag{C 6}$$

To match with I_1, the behaviour of solutions as $z\to\infty$ becomes

$$\psi_0 = A_0\,\mathrm{e}^{-\alpha_0}, \quad \tilde{\psi}_0 = D_0,$$

$$\psi_1 \sim -\alpha_0\,\mathrm{e}^{-\alpha_0}A_0\,z, \quad \psi_2 \sim \tfrac{1}{2}\alpha_0^2 A_0\,\mathrm{e}^{-\alpha_0}z^2,$$

$$\tilde{\psi}_1 \sim D_1 z+D_2 z\ln z, \quad \hat{\psi}_0 \sim -D_2 z. \tag{C 7}$$

The basic flow in II is

$$\bar{u}_{\mathrm{II}} = \epsilon(L+z)\,\lambda+\lambda_2\epsilon^2(L+z)^2+\gamma\epsilon^2\,\mathrm{e}^{-z}+\ldots. \tag{C 8}$$

Substitution of (C 6), (C 8) into the Rayleigh equation, yields the equations

$$(\lambda z-c_0)\,\psi_0'' = 0, \quad (\lambda z-c_0)\,\psi_1''-c_1\,\psi_0'' = 0, \tag{C 9a, b}$$

$$(\lambda z-c_0)\,\psi_2''-c_1\,\psi_1-c_2\,\psi_0'' = (\lambda z-c_0)\,\alpha_0^2\,\psi_0. \tag{C 9c}$$

The solutions of (C 9*a–c*) that are consistent with those in I_1 according to (C 7) are

$$\psi_0 = A_0\,\mathrm{e}^{-\alpha_0}, \quad \psi_1 = -\alpha_0\,\mathrm{e}^{\alpha_0}A_0\,z, \quad \psi_2 = \tfrac{1}{2}\alpha_0^2 A_0\,\mathrm{e}^{-\alpha_0}z^2. \tag{C 10}$$

At $O(L)$ and $O(1)$ respectively we have

$$(\lambda z-c_0)\,\tilde{\psi}_0'' = \lambda_2\,\psi_1''+2\lambda_2 z\psi_0 = 0, \tag{C 11a}$$

$$(\lambda z-c_0)\,\tilde{\psi}_1''-c_1\,\tilde{\psi}_0''+\lambda_2\,\psi_2''+\lambda_2 z\psi_1''+\lambda_2 z^2\psi_0''-\alpha_0^2\lambda_2\,\psi_0+\gamma\,\mathrm{e}^{-z}\,\psi_0'' = (2\lambda_2+\gamma\,\mathrm{e}^{-z})\,\psi_0. \tag{C 11b}$$

The solution of (C 11a) subject to (C 7) is $\tilde{\psi}_0 = D_0$, while the equation for $\tilde{\psi}_1$ becomes

$$\tilde{\psi}_1 = \frac{(2\lambda_2 + \gamma \mathrm{e}^{-z}) A_0 \mathrm{e}^{-\alpha_0}}{\lambda(z - c_0/\lambda)}. \tag{C 11c}$$

Finally, the equation for $\hat{\psi}_0$ is obtained from a balance of $O(\ln L)$ terms in the Rayleigh equation and is, together with its solution that satisfies matching requirements with region I_1,

$$(\lambda z - c_0)\hat{\psi}_0 = 0, \quad \hat{\psi}_0 = -D_2 z.$$

Equation (C 11c) is free of singularities at $z = c_0/\lambda$ if

$$c_0 = -\lambda \ln\left(\frac{-2\lambda_2}{\gamma}\right). \tag{C 12}$$

With $\tilde{\psi}_1$ smooth, higher-order corrections in c that are real can be found. The expression (C 12) gives a correction to the leading-order terms of the wave speed and it is necessary to show that eigensolutions can be found in the remaining regions, I_2 and III, that match uniformly to those in II and I_1.

It is easy to show that the solution $\tilde{\psi}_1$ matches with that in I_1 as $z \to \infty$. Consider now (C 11c) as $z \to -\infty$, in order to match solutions between regions II and I_2. $\tilde{\psi}_1$ contains exponentially large terms in this case; in fact

$$\tilde{\psi}_1 \sim -\frac{\gamma A_0 \mathrm{e}^{-\alpha_0} \mathrm{e}^{\zeta}}{\lambda \zeta} + O\left(\frac{\mathrm{e}^{\zeta}}{\zeta^2}\right) \quad \text{as} \quad \zeta \to \infty \quad (\zeta = -z).$$

Writing this in terms of the local variable of region I_2 ($y = \epsilon L Y$), $\tilde{\psi}_1$, implies a contribution of $O(\epsilon^{Y-1}/L)$ terms to the solution in region I_1. It is found, therefore, that the correct expansion to be formed in I_2 is

$$\psi_{\mathrm{I}_2} = \Psi_0 + \epsilon L \Psi_1 + \ldots + \frac{\epsilon^Y}{L}(\bar{\psi}_0 + L^{-1}\bar{\psi}_1 + \ldots) + \text{h.o.t.} \tag{C 13}$$

In (C 13) Ψ_0 is given by (C 4a) and Ψ_1 satisfies (C 3). At $O(\epsilon^{Y-1})$ the Rayleigh equation implies

$$\Psi_0 = -\frac{\gamma A_0 \mathrm{e}^{-\alpha_0 Y}}{\lambda(1 - Y)}$$

which matches with the contribution of $\tilde{\psi}_1$ in II. The solution of (C 3) in I_2 is not the same as that in I_1, owing to the lifting of the boundary condition at infinity; it can be found as before and its behaviour analysed as $Y \to 1-$, to give

$$\Psi_1^{(\mathrm{I}_2)} \sim \hat{D}_0 + s\hat{D}_1 + s \ln s \hat{D}_2 + \ldots \quad \text{as} \quad s \to 0 \quad (s = 1 - Y),$$

where D_0, D_1, D_2 involve the unknowns α_1 and B_1. Complete matching of solutions through II to I_1 gives

$$\hat{D}_0 = D_0, \quad \hat{D}_1 = -D_1$$

which can be used to find α_1.

It remains to construct solutions inside the Goldstein layer. Here $y = \epsilon Z$, $Z = O(1)$ and

$$\psi_{\mathrm{III}} = \hat{\Psi}_0 + L^{-1}\hat{\Psi}_1 + \ldots + \text{other terms}.$$

The Rayleigh equation at $O(L\epsilon^{-1})$ and $O(\epsilon^{-1})$ respectively gives

$$-\lambda \hat{\Psi}_0'' = 0, \quad -\lambda \hat{\Psi}_1'' + (F - c_0)\hat{\Psi}_0'' = F''\hat{\Psi}_0. \tag{C 14a, b}$$

The solution of (C 14*a*) that satisfies the symmetry conditions and matches with that in I_2 is $\hat{\Psi}_0 = A_0$, and the solution of (C 14*b*) together with its behaviour for large Z is

$$\hat{\Psi}_1 = -\frac{F(Z)A_0}{\lambda} + a_1, \quad \hat{\Psi}_1 \sim -\frac{A_0}{\lambda}(\lambda Z + A_G + \gamma e^{-Z}) + a_1. \tag{C 15}$$

In (C 15) above, a_1 is a constant to be determined; it can be found by consideration of the contributions from Ψ_0 and $\epsilon^Y \bar{\psi}_0$ from I_2 as $Y \to 0+$. This gives

$$a_1 = \frac{A_0 A_G}{\lambda}, \quad \alpha_0 = 1.$$

Higher-order solutions can be obtained in a similar manner.

REFERENCES

Betchov, R. & Criminale, W. O. 1967 *Stability of Parallel Flows*. Academic.

Cebeci, T., Thiele, F., Williams, P. G. & Stewartson, K. 1979 On the calculation of symmetric wakes. I. Two-dimensional flows. *Numer. Heat Transfer* **2**, 35–60.

Curle, N. 1957 On hydrodynamic stability in unlimited fields of viscous flow. *Proc. R. Soc. Lond.* A **238**, 489–501.

Drazin, P. G. & Howard, L. N. 1962 The stability to long waves of parallel inviscid flow. *J. Fluid Mech.* **14**, 257–283.

Drazin, P. G. & Howard, L. N. 1966 Hydrodynamic stability of parallel flow of inviscid fluid. *Adv. Appl. Mech.* **9**, 1–89.

Drazin, P. G. & Reid, W. H. 1981 *Hydrodynamic Stability*. Cambridge University Press.

Gaster, M. 1968 Growth of disturbances in both space and time. *Phys. Fluids* **11**, 723–727.

Goldstein, S. 1930 Concerning some solutions of the boundary layer equations in hydrodynamics. *Proc. Camb. Phil. Soc.* **26**, 1–30.

Hollingdale, S. H. 1940 Stability and configuration of the wakes produced by solid bodies moving through fluids. *Phil. Mag.* (7) **29**, 209–257.

Keller, H. B. & Cebeci, T. 1971 *2nd Intl Conf. Num. Meth. Fluid Dyn., Berkeley*, p. 92. Springer.

Lin, C. C. 1955 *The Theory of Hydrodynamic Stability*. Cambridge University Press.

McKoen, C. H. 1957 *Aero. Res. Coun., Lond., Rep.* 303.

Mattingly, G. E. & Criminale, W. O. 1972 The stability of an incompressible wake. *J. Fluid Mech.* **51**, 233–272.

Messiter, A. F. 1970 Boundary layer flow near the trailing edge of a flat plate. *SIAM J. Appl. Maths* **18**, 241–257.

Miksad, R. W., Jones, F. L., Kim, Y. C. & Khandra, L. 1982 Experiments on the role of amplitude and phase modulation during transition to turbulence. *J. Fluid Mech.* **123**, 1–29.

Miksad, R. W., Jones, F. L. & Powers, E. J. 1983 Measurements of nonlinear interactions during natural transition of a symmetric wake. *Phys. Fluids* **26**, 1402–1409.

Papageorgiou, D. T. & Smith, F. T. 1988 Theoretical investigation of the nonlinear instability of the wake behind a flat plate placed parallel to a uniform stream. *Proc. R. Soc. Lond.* A **419**, 1–28.

Sato, H. & Kuriki, K. 1961 The mechanism of transition in the wake of a thin flat plate placed parallel to a uniform flow. *J. Fluid Mech.* **11**, 321–352.

Smith, F. T. 1974 Boundary layer flow near a discontinuity in wall conditions. *J. Inst. Maths Applics* **13**, 127–145.

Stewartson, K. 1969 On the flow near the trailing edge of a flat plate-II. *Mathematika* **16**, 106–121.

Taneda, S. 1965 The stability of two-dimensional laminar wakes at low Reynolds numbers. *J. Phys. Soc. Japan* **18**, 288.

Tollmien, W. 1935 General stability criterion of laminar velocity distributions (translated from the German original). *Tech. Memo. Natl Adv. Comm. Aero. Wash.* 792.